

Electromechanical modeling of eye fatigue detecting using flexible piezoelectric sensors

Chaofeng LU^{1,2,3*}, Shuang WU¹, Yangyang ZHANG¹ & Yangkun DU⁴

¹College of Civil Engineering and Architecture, Zhejiang University, Hangzhou 310058, China;

²Key Laboratory of Soft Machines and Smart Devices of Zhejiang Province, Zhejiang University, Hangzhou 310027, China;

³Soft Matter Research Center, Zhejiang University, Hangzhou 310027, China;

⁴Department of Engineering Mechanics, Zhejiang University, Hangzhou 310027, China

Received 21 January 2018/Revised 28 February 2018/Accepted 21 March 2018/Published online 15 May 2018

Abstract Eye fatigue has attracted significant interest due to its potential harm to human daily activities. An ultrathin flexible piezoelectric sensor was currently designed and fabricated to detect eye fatigue by deforming together with the eyelid epidermis. Herein we develop a theoretical model to illustrate the correlation between the eyelid motion and the signals output by the piezoelectric sensor. The theoretical predictions on the eyelid motion based on the measured electrical output agree well with the in vivo observations in experiment. A simple scaling law is established to evaluate the impacts of different parameters on the function ability of the flexible piezoelectric sensor. The results may provide useful guidelines for designing and optimizing similar devices for alike biological motions.

Keywords electromechanical model, flexible piezoelectric sensors, eye fatigue monitoring, scaling law, micromechanics

Citation Lu C F, Wu S, Zhang Y Y, et al. Electromechanical modeling of eye fatigue detecting using flexible piezoelectric sensors. *Sci China Inf Sci*, 2018, 61(6): 060417, <https://doi.org/10.1007/s11432-018-9397-0>

1 Introduction

Eye fatigue is a commonly recognized healthcare problem that can possibly cause serious harm to human safety and properties [1–3]. It has been studied by researchers from multiple disciplines, e.g., medical fields, physiology, and transportation. Different approaches were taken to detect eye fatigue through physiological signals such as electroencephalogram (EEG), electrocardiogram (ECG), or pulse rate [4, 5]. These methods require sophisticated sensing modules and rigid test environments which is not suitable for situations that require the device to be portable and small in size, e.g., a driver's seat. Meanwhile, external behaviors like blinking and nodding have also been proved to be associated with human fatigue status [6]. Research outcomes of computer vision have been applied to fatigue detecting based on blinking behavior [7–9]. For being more convenient and simple structured, similar fatigue detecting camera have been employed in intelligent cars [9], whereas the accuracy of such device can be damped by driver's unpredictable head move or bad visibility at night. Concerning the balance between accuracy and conveniences, a new approach was developed that exploits the novel technology of epidermal electronics [10–12]. Based on this idea, an ultrathin flexible piezoelectric sensor was currently designed and fabricated as an innovative solution to real-time eye fatigue detecting (Figure 1) [13]. As shown in Figure 1(b), the sensor

* Corresponding author (email: lucf@zju.edu.cn)

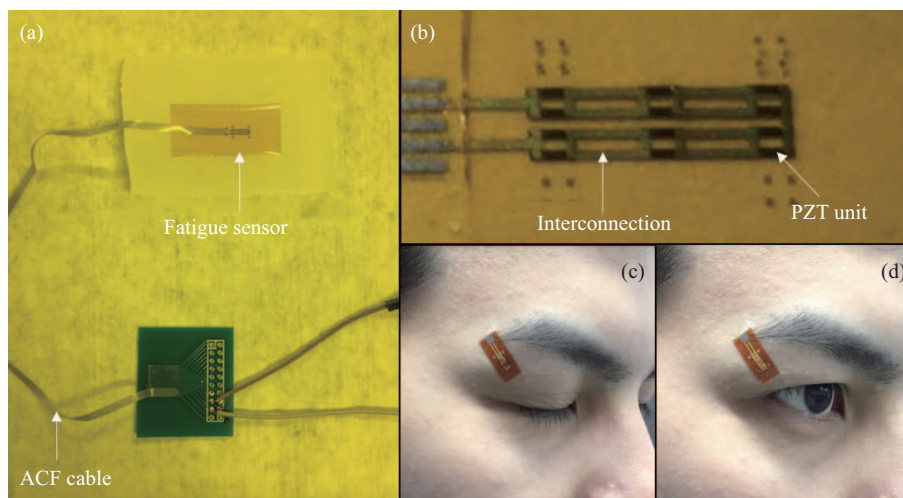


Figure 1 (Color online) (a) Photograph of a piezoelectric fatigue sensor connected with ACF cable; (b) photograph of the core functioning part of the piezoelectric fatigue sensor; (c) and (d) photographs of a volunteer wearing the sensor with eyelid closed and open.

contains an array of lead zirconium titanate (PZT) nanoribbons integrated on flexible substrate which is directly attached to upper eyelid. The PZT ribbon of the sensor is a sandwich-layer structure where the thin PZT films are wrapped between upper and lower electrodes (Figure 2(a)). By conformally deforming with the eyelid during eye blink, the sensor is able to detect eyelid motion precisely and reveal human's fatigue state [13]. The output voltage signal is collected by an oscilloscope which is connected with the piezoelectric sensor using an anisotropic conductive film (ACF) cable. This sensor has great utility potential for its extremely thin and flexible nature without any distraction to the eyelid. In addition, it is a self-powered system that can operate without battery charging.

In this paper, a theoretical model is developed to illustrate the electromechanical behavior within the system. The correlations between the output voltage and the sensor strain, therefore, the eyelid strain, can perfectly predict the motion of eyelid movement basing on the output signal of the sensor. Comparisons are made between the theoretical predictions and the experimental observations to validate the theoretical formulations. A simple scaling law is established that combines various geometrical, material, circuit and mechanical load parameters to reveal the underlying detecting mechanism of the sensor. The results presented here may provide a useful guideline for the design and optimization of similar devices for detecting biological motions.

2 Theoretical formulations and discussion

Since the sensor is perfectly bonded with human epidermis, we suppose that the polyimide (PI) substrate and eyelid epidermis deform conformally without any slippage. When the eyelid contract during blinking, the device together with the eyelid epidermis is deformed into a sinusoidal arch shape with the middle part buckling up. Though the substratum of skin and muscle has a very complicated mechanism, we can simplify the system to a double layered film with distributed PZT nanoribbons under compression strain. The fabricated sensor (length 2 cm) is composed of an array of PZT nanoribbons (thickness 1.5 μm) which are integrated on a PI substrate (thickness 30 μm). Hence the contribution from PZT nanoribbons to the overall bending rigidity of the whole system is negligible. The out of plane displacement of the composite layered system in post-buckling may take the form (Figure 2(b)) [14]

$$w = \frac{A}{2} \left[1 + \cos \left(\frac{2\pi x}{L_0} \right) \right], \quad \left(|x| \leq \frac{L_0}{2} \right), \quad (1)$$

where A and L_0 are respectively the amplitude of buckle and the initial length of the device. Here, we neglect the contribution of the energies related to the PZT ribbons, i.e., their bending energy, membrane

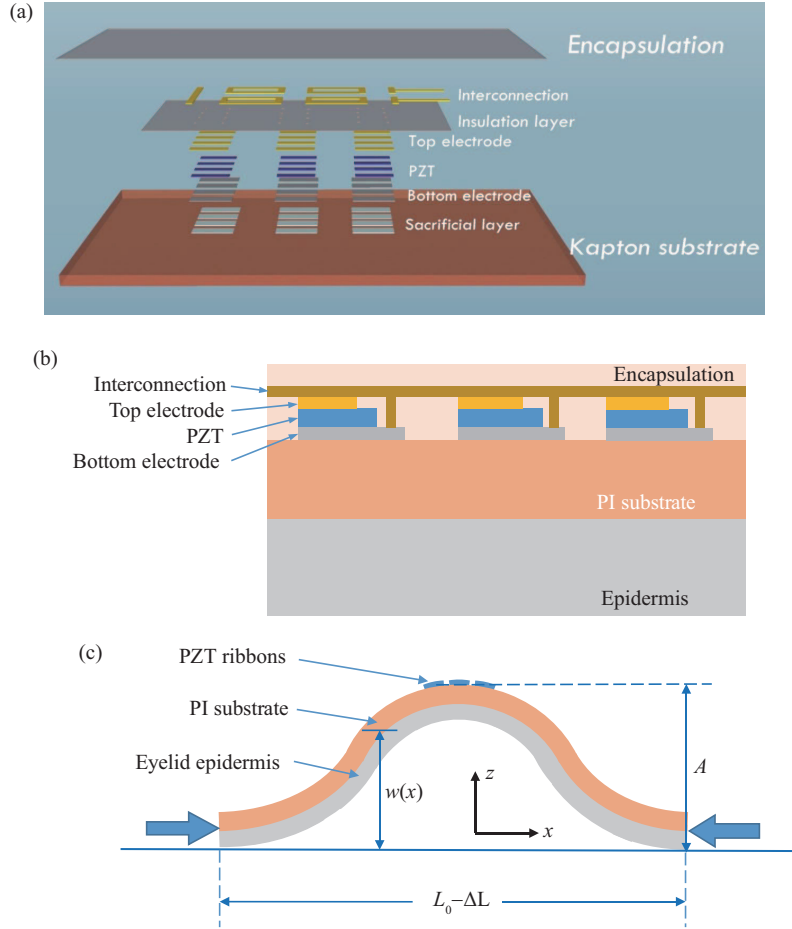


Figure 2 (Color online) (a) Schematic diagram of the piezoelectric device; (b) profile diagram of the central part of piezoelectric device; (c) schematic diagram of the piezoelectric device conformally deforming with the eyelid epidermis.

energy, and that electromechanical energy. Then the energy of the whole system can be expressed as [15, 16]

$$U_{\text{total}} = \frac{\bar{E}h^3\pi^4 A^2}{12L_0^3} + \frac{1}{2}\bar{E}hL_0 \left(\frac{\pi^2 A^2}{4L_0^2} - \frac{\Delta L}{L_0} \right)^2, \quad (2)$$

where \bar{E} and h are respectively the Young's modulus and thickness of the double layered film, and ΔL is the end-to-end displacement of the device. Employing the principle of minimal potential energy, we get, $\partial U_{\text{total}}/\partial A = 0$, then the amplitude of the buckle can be solved as

$$A = \sqrt{\frac{4\Delta L \cdot L_0}{\pi^2} - \frac{4h^3}{3}} \approx \frac{2}{\pi} \sqrt{\Delta L \cdot L_0}. \quad (3)$$

Using the equilibrium condition of bending moment (or equivalent curvature) at the joint cross section of the layered film with and without PZT ribbons, the axial normal strain of the PZT ribbon is given as

$$\varepsilon_{p,x} = -\beta z_p \frac{d^2 w}{dx^2} = 4\pi\beta \frac{z_p}{L_0} \sqrt{\frac{\Delta L}{L_0}} \cos\left(\frac{2\pi x}{L_0}\right), \quad (4)$$

where $\beta = \bar{EI}/E'I'$ is the bending rigidity ratio of the double layer substrate (\bar{EI}) to the composite section integrated with PZT ribbons ($E'I'$), and z_p is the distance from the center of the PZT ribbons to the neural axis of the composite substrate. Since the PZT ribbons are extremely small in length (760 μm) compared to the entire device and approximately located at the center of the device, we may take $x/L_0 \approx 0$ in (4).

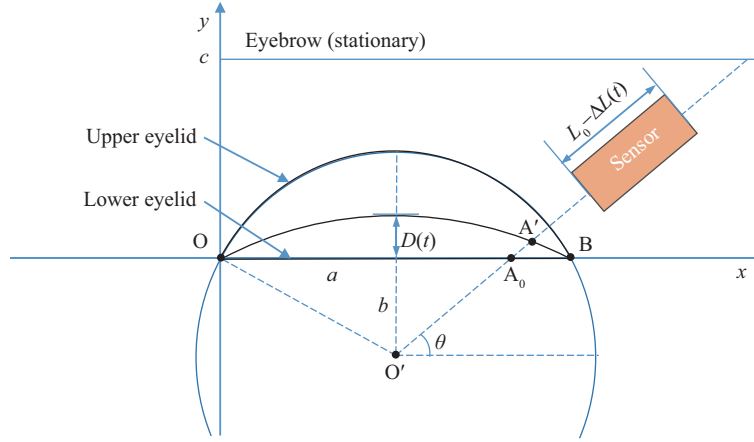


Figure 3 (Color online) Schematic of geometrical relationship between the eyelid distance and end-to-end displacement of the sensor.

For the current ultrathin composite film system, the constitutive equations for the PZT ribbon read [17]

$$D_z = \bar{e}_{31}\varepsilon_{p,x} + \bar{\mu}_{33}\frac{V}{h_p}, \quad (5)$$

where V is the voltage drop across the thickness (h_p) of an individual PZT ribbon, while $\bar{c}_{11} = c_{11} - c_{13}^2/c_{33}$, $\bar{e}_{31} = e_{31} - c_{13}e_{33}/c_{33}$, and $\bar{\mu}_{33} = \mu_{33} + e_{33}^2/c_{33}$ are respectively the effective modulus, effective piezoelectric and dielectric constants. Substituting (4) into (5) and integrating the electrical displacement across the effective area of an individual PZT ribbon, the electrical charge collected by one ribbon is obtained as

$$Q = 4\pi\beta\frac{\bar{e}_{31}z_p A_p}{L_0}A + \frac{\bar{\mu}_{33}A_p}{h_p}V, \quad (6)$$

where the A_p is the effective area of each individual PZT ribbon to collect electric charge.

For the application of sensing, multiple such PZT ribbons were connected in series and parallel. Supposing the number of parallel connected PZT ribbons is n_p , while the number of series is n_s , the total voltage output is $V_{\text{total}} = n_s V$, and the electrical current is $I = V_{\text{total}}/R$, where R is the electric resistance of the circuit. Combining these equations above gives the following first-order differential equation.

$$\frac{dV_{\text{total}}}{dt} + \frac{n_s h_p}{\bar{\mu}_{33} n_p A_p R} V_{\text{total}} = -4\pi\beta\frac{n_s \bar{e}_{31} z_p h_p}{\bar{\mu}_{33} L_0} \frac{dA}{dt}. \quad (7)$$

The general solution is

$$V_{\text{total}}(t) = -4\pi\frac{n_s \bar{e}_{31} h_p z_p}{\bar{\mu}_{33}} \exp\left(-\frac{n_s h_p}{\bar{\mu}_{33} n_p A_p R} t\right) \int_0^t \exp\left(\frac{n_s h_p}{\bar{\mu}_{33} n_p A_p R} t'\right) \times \frac{dA}{dt'} dt', \quad (8)$$

where the initial condition $V_{\text{total}}(0) = 0$ is applied. This solution will approach a periodic function as $t \rightarrow \infty$ if the end-to-end displacement is a periodic function (e.g., eye blinking).

Combining (3) and (8), we may derive the relation between the output voltage V_{total} and the end-to-end displacement ΔL of the sensor. In order to illustrate further the eyelid motion, it is necessary to establish the relation between the distance of upper and lower eyelids and the end-to-end displacement of the sensor. The actual movement and deformation of eyelid epidermis are very complicated, we assume that the upper eyelid is in a circular arch shape when open, while the lower eyelid is in a straight line and the eyebrow remains fixed during blinking (Figure 3). Then, the eyelid distance $D(t)$, that is defined as the distance between the upper and lower eyelids at the center point, may be determined by

$$D(t) = \frac{(\sqrt{a^2 + b^2} - b) \cdot c}{(\sin(\theta) \sqrt{a^2 + b^2} - b) L_0} \Delta L(t), \quad (9)$$

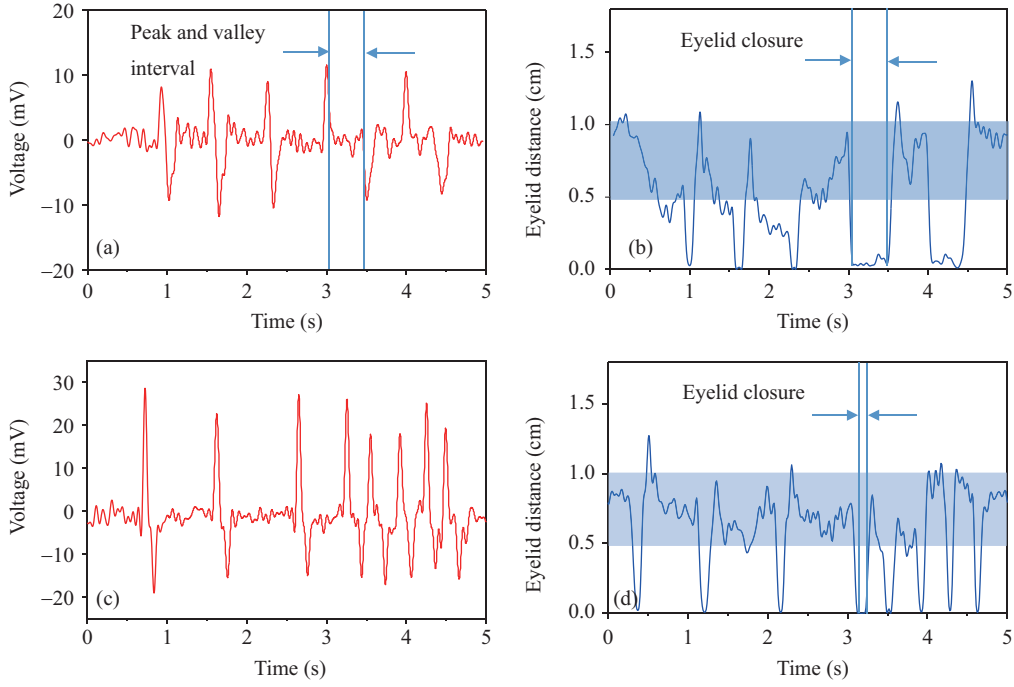


Figure 4 (Color online) (a) and (c) output voltage signals collected from in vivo test of a volunteer wearing the sensor; (b) and (d) theoretical predictions of the eyelid distance based on the measured data in (a) and (c).

where a , b , c and θ are geometric parameters as defined in Figure 3. Combining (3), (8) and (9), we can obtain the relation between the output voltage and the eyelid distance.

In experiment, material, geometrical, and circuit properties of the sensor are $\bar{e}_{31} = -40.5 \times 10^{-12}$ C/N, $\bar{\mu}_{33} = 8.854 \times 10^{-8}$ F/m [18, 19], $A_p = 1.216 \times 10^{-7}$ m², $h_p = 1.5$ μ m, $a = 1.6$ cm, $b = 1.0$ cm, $c = 2.0$ cm, $L_0 = 2.0$ cm, $\theta = 35^\circ$, $z_p = 9.642$ μ m, $\beta = 0.793$ [20, 21], $R = 10$ M Ω , $n_s = 6$ and $n_p = 2$. Based on the measured voltage signals from the in vivo test (Figure 4(a) and (c)), the calculated eyelid distance may predict very well with the eyelid motions that are observed in experiment.

The voltage signals in Figure 4(a) reveals three periods of normal eye blinks with very short closure state while the subsequent two blinks have a wider zero platform between peak and valley voltage. This interval represents the time period of eyelid closure as the theoretical prediction (Figure 4(b)). It is a very critical parameter because the ratio of closure period within a blink cycle is of great concern especially in fatigue driving research [22]. The larger this ratio is, the more it is likely to induce mass traffic accidents. A clear acceleration of blinking frequency is observed in experiment and is revealed by the measure voltage in Figure 4(c). From medical perspective, it is a self-wakening phenomenon, which involuntarily appears when people get tired [23, 24]. This phenomenon of eyelid motion is precisely captured by the theoretical prediction on the eyelid distance in Figure 4(d).

Another significant parameter for eye fatigue detecting is the opening level of eyelid that is marked as shaded parts in Figure 4(b) and (d). It is obvious that the opening level of Figure 4(d) is much larger than that of Figure 4(b), suggesting a more lucid mental state that is also observed in experiment. The slope of the dropping part of the eyelid distance curve is generally larger than that of the rising part (Figure 4(b) and (d)). This phenomenon matches well with big data because the closing of eyelid is normally two to three times faster than its opening [25].

As observed from the experimental measurements (Figure 4(a) and (c)), the output voltage is in an order of 10 mV that may require a scope with relative high sensitivity. It is noteworthy that this output signal has been filtered by a 15 Hz FFT filter because the raw data inevitably contains some noise signal induced by the external interference current. Based on our theoretical formulations, we may also establish an optimized design of the device so that the output voltage increases by several orders but without adverse effects to the eyelid epidermis. The output voltage in (8) contains a bunch

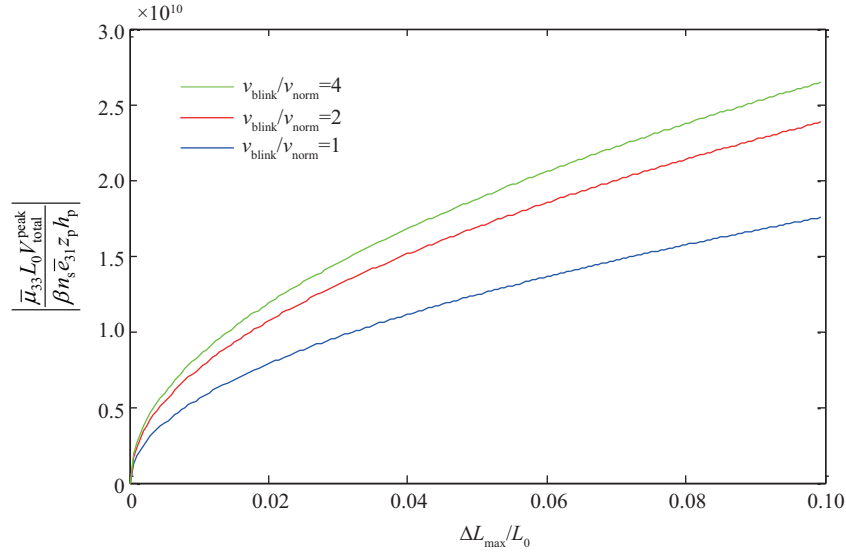


Figure 5 (Color online) Dependence of the normalized peak voltage on the normalized end-to-end displacement of the sensor under different normalized blinking speed.

of material parameters (e.g., piezoelectric constant $\bar{\epsilon}_{31}$, dielectric constant $\bar{\mu}_{33}$, Young's modulus E), structural parameters (e.g., distance z_p , bending rigidities $\bar{E}I$ and $E'I'$), geometric parameters (e.g., device length L_0 , thickness and effective area of the PZT h_p and A_p , and thickness of the substrate h_s), circuit parameters (e.g., electrical resistance R , number of PZT ribbons n_p connected in parallel in one module and number of modules n_s connected in series). To evaluate the effects of these complicated parameters, a simple scaling law is established.

Introducing the intrinsic time scale $t_0 = (\bar{\mu}_{33} n_p A_p R) / n_s h_p$, the normalized time $\tau = t/t_0$, and the normalized period $\bar{T} = T/t_0$, the normalized output voltage is derived as

$$\frac{\bar{\mu}_{33} L_0 V_{\text{total}}}{\beta n_s \bar{\epsilon}_{31} z_p h_p} = f\left(\frac{t}{t_0}, \frac{T}{t_0}, \frac{\Delta L}{L_0}\right), \quad (10)$$

which gives the scaling law for the detecting of eye fatigue. It suggests that the normalized output voltage depend only on two parameters, the normalized eyeblink period and the normalized isosceles trapezoid function $\Delta L/L_0$ with respect to t/t_0 . In the function $\Delta L/L_0$, the speed of blink, v_{blink} , and the maximal opening of the eyelid have significant impact on the peak value of the output signal $V_{\text{total}}^{\text{peak}}$. From theoretical predictions in Figure 4(d), a normal ΔL_{max} lies between 0.5 and 1.0 cm. According to clinical investigation [25], normal time period of eyelid sliding down takes around 0.05 s, while the sliding up period takes around 0.15 s. Here we choose three different blinking speeds to reveal the impact on the output voltage of sensor.

The correlation between the normalized peak output voltage $\frac{\bar{\mu}_{33} L_0 V_{\text{total}}^{\text{peak}}}{\beta n_s \bar{\epsilon}_{31} z_p h_p}$ and the normalized maximal end-to-end displacement $\frac{\Delta L_{\text{max}}}{L_0}$ of the sensor for various values of $\frac{v_{\text{blink}}}{v_{\text{blink}}^{\text{normal}}}$ are presented in Figure 5 for $\frac{\bar{\mu}_{33} n_p A_p R}{n_s h_p T} = 0.024$, where $\frac{v_{\text{blink}}}{v_{\text{blink}}^{\text{normal}}} = 1$ indicates that the blinking speed equals the normal blinking speed $v_{\text{blink}}^{\text{normal}}$ of healthy normal state. The monotonically increasing curves suggest that, keeping the layouts of PZT moduli, larger end-to-end displacement of the device (or eyelid distance) and larger blinking speed of the eyelid produces larger peak output voltage. Figure 6 presents the scaling dependence of the normalized peak voltage on the combined parameter $\frac{\bar{\mu}_{33} n_p A_p R}{n_s h_p T}$ for $\frac{\Delta L_{\text{max}}}{L_0} = 0.05$ (corresponding to normal blinking). The normalized peak voltage increases monotonically and tends to saturate as the $\frac{\bar{\mu}_{33} n_p A_p R}{n_s h_p T}$ reaches a relative large value. This is not difficulty to understand since the output voltage is zero when the circuit is shorted but approaches to the open circuit voltage as the electric resistance increases. This indicates that increasing the electrical resistance R may magnify the output voltage by several times. For example, the current device and detecting circuits ($R = 10 \text{ M}\Omega$) yield an output peak voltage of about

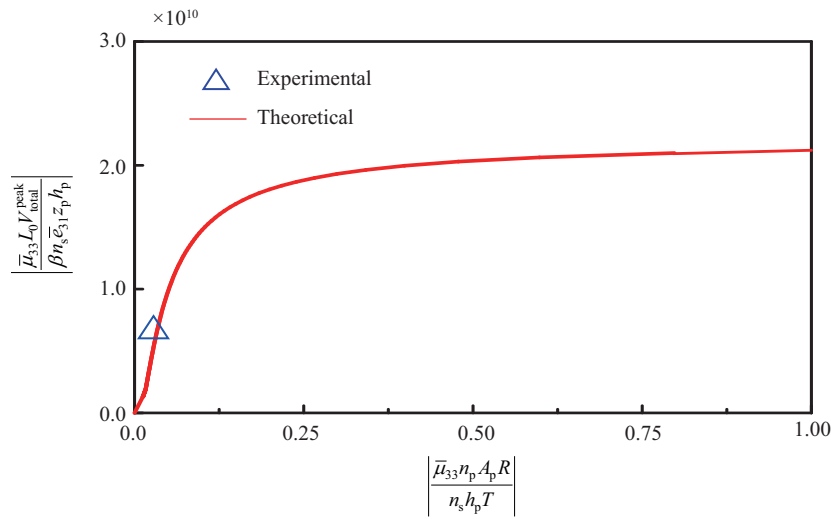


Figure 6 (Color online) Scaling law for the normalized peak voltage and the normalized parameter $\bar{\mu}_{33} n_p A_p R / n_s h_p T$.

15 mV, but the value may increase up to 31.95 mV if the electric resistance is replaced by $R = 100 \text{ M}\Omega$. This scaling curve may also provide a design guideline for maximizing the output voltage. For example, the output voltage is inversely proportional to the device length, which indicates that decreasing the device length by a half may double the output voltage. In addition, increasing the overall effective area of the PZT ribbons in on module, i.e., $n_p A_p$, may also magnify the output voltage signal significantly. For example, if $n_p A_p$ increases by one order, the output voltage may be magnified by 4.35 times.

3 Conclusion

In summary, an electromechanical model was developed to predict the function of an ultrathin flexible piezoelectric sensor for monitoring eye fatigue. The theoretical calculations can perfectly predict eyelid motion based on the output voltage of the sensor. From the calculated eyelid distance curve, some critical parameters, e.g., the blinking frequency, opening level of eyelid, eye closure period, and opening speed, can be extracted for fatigue state assessment. Some specific parameters and phenomenon match well with clinical investigations, thus demonstrates the feasibility and reliability of the theoretical model. Finally, a simple scaling law was established to illustrate the impacts of eyelid motion on the peak value of output signals, which may help to guideline design of this type of device for bio-signals.

Acknowledgements This work was supported by National Natural Science Foundation of China (Grant Nos. 11322216, 11621062).

References

- 1 Connor J, Norton R, Ameratunga S, et al. Driver sleepiness and risk of serious injury to car occupants: population based case control study. *BMJ*, 2002, 324: 1125
- 2 Huang J, Wang Y, Fu Z Y, et al. Fatigue among clinicians and the safety of patients. *Chinese Medical Ethics*, 2008, 347: 1249–1255
- 3 Lal S K L, Craig A. A critical review of the psychophysiology of driver fatigue. *Biol Psychol*, 2001, 55: 173–194
- 4 Saito S. Does fatigue exist in a quantitative measurement of eye movements? *Ergonomics*, 1992, 35: 607–615
- 5 Wu J D, Chen T R. Development of a drowsiness warning system based on the fuzzy logic images analysis. *Expert Syst Appl*, 2008, 34: 1556–1561
- 6 Dinges D F, Grace R. Perclos: a valid psychophysiological measure of alertness as assessed by psychomotor vigilance. *Tech Brief*, 1998, 35: 607–615
- 7 Divjak M, Bischof H. Eye blink based fatigue detection for prevention of computer vision syndrome. In: *Proceedings of Conference on Machine Vision Application*, Yokohama, 2009. 350–353
- 8 Zhang Z T, Zhang J S. A new real-time eye tracking for driver fatigue detection. In: *Proceedings of the 6th International Conference on Telecommunications*, Chengdu, 2006. 8–11

- 9 Ji Q, Zhu Z, Lan P. Real-time noninvasive monitoring and prediction of driver fatigue. *IEEE Trans Veh Technol*, 2004, 53: 1052–1068
- 10 Martirosyan N, Kalani M Y. Epidermal electronics. *Science*, 2011, 333: 485–486
- 11 Wang S D, Li M, Wu J, et al. Mechanics of epidermal electronics. *J Appl Mech*, 2012, 79: 031022
- 12 Yeo W H, Kim Y S, Lee J, et al. Multifunctional epidermal electronics printed directly onto the skin. *Adv Mater*, 2013, 25: 2773–2778
- 13 Lu C F, Wu S, Lu B W, et al. Ultrathin exible piezoelectric sensors for monitoring eye fatigue. *J Micromech Microeng*, 2018, 28: 2
- 14 Jiang H, Khang D Y, Song J, et al. Finite deformation mechanics in buckled thin films on compliant supports. *Proc Natl Acad Sci USA*, 2007, 104: 15607–15612
- 15 Jiang H, Sun Y, Rogers J A, et al. Mechanics of precisely controlled thin film buckling on elastomeric substrate. *Appl Phys Lett*, 2007, 90: 133119
- 16 Zhang Y Y, Chen Y S, Lu B W, et al. Electromechanical modeling of energy harvesting from the motion of left ventricle in closed chest environment. *J Appl Mech*, 2016, 83: 061007
- 17 Ding H J, Chen W Q. 3 dimensional problems of piezoelectricity. *Nova Biomed*, 2001, 532
- 18 Lente M H, Eiras J A. Interrelationship between self-heating and ferroelectric properties in PZT ceramics during polarization reorientation. *J Phys-Condens Matter*, 2000, 12: 5939–5950
- 19 Mitchell J A, Reddy J N. A refined hybrid plate theory for composite laminates with piezoelectric laminae. *Int J Solids Struct*, 1995, 32: 2345–2367
- 20 Agache P G, Monneur C, Leveque J L, et al. Mechanical properties and Young's modulus of human skin in vivo. *Arch Dermatol Res*, 1980, 269: 221–232
- 21 Takema Y, Yorimoto Y, Kawai M, et al. Age-related changes in the elastic properties and thickness of human facial skin. *Br J Dermatol*, 1994, 131: 641–648
- 22 Eriksson M, Papanikolopoulos N P. Driver fatigue: a vision-based approach to automatic diagnosis. *Transpation Res Part C-Emerg Technol*, 2001, 9: 399–413
- 23 Schmidtke K, Büttner-Ennever J A. Nervous control of eyelid function. *Brain*, 1992, 115: 227–247
- 24 von Cramon D, Schuri U. Blink frequency and speech motor activity. *Neuropsychologia*, 1980, 18: 603–606
- 25 Evinger C, Manning K A, Sibony P A. Eyelid movements. mechanisms and normal data. *Invest Ophth Vis Sci*, 1991, 32: 387–400